Dynamics of Liquids, Molecules, and Proteins Measured with Ultrafast 2D IR Vibrational Echo Chemical Exchange Spectroscopy

M.D. Fayer

Department of Chemistry, Stanford University, Stanford, California 94305;
email: fayer@stanford.edu

Annu. Rev. Phys. Chem. 2009. 60:21–38

First published online as a Review in Advance on October 13, 2008

The *Annual Review of Physical Chemistry* is online at physchem.annualreviews.org

This article's doi:
10.1146/annurev-physchem-073108–112712

0066-426X/09/0505-0021$20.00

Key Words

solute-solvent complex dynamics, carbon-carbon single-bond isomerization dynamics, protein structural substate switching dynamics

Abstract

A wide variety of molecular systems undergo fast structural changes under thermal equilibrium conditions. Such transformations are involved in a vast array of chemical problems. Experimentally measuring equilibrium dynamics is a challenging problem that is at the forefront of chemical research. This review describes ultrafast 2D IR vibrational echo chemical exchange experiments and applies them to several types of molecular systems. The formation and dissociation of organic solute-solvent complexes are directly observed. The dissociation times of 13 complexes, ranging from 4 ps to 140 ps, are shown to obey a relationship that depends on the complex's formation enthalpy. The rate of rotational *gauche-trans* isomerization around a carbon-carbon single bond is determined for a substituted ethane at room temperature in a low viscosity solvent. The results are used to obtain an approximate isomerization rate for ethane. Finally, the time dependence of a well-defined single structural transformation of a protein is measured.

1. INTRODUCTION

A vast amount of chemistry occurs at or near room temperature in the ground electronic states of molecules. From synthetic organic chemistry to biological chemistry, chemical processes occur on fast timescales. Although the rate of an overall process may be slow, key events on the molecular level are fast. For example, in a second-order reaction, the reaction rate can be controlled by the diffusion of the species into contact, but the actual reactive event occurs on a very fast timescale. The binding of a substrate to an enzyme can be very slow, but the structural changes of the enzyme or the reaction of the substrate once the substrate finds its way into the binding site can be very fast.

One challenge is to be able to directly observe fast timescale thermal equilibrium chemical events without changing the system's equilibrium behavior. Ultrafast two-dimensional infrared (2D IR) vibrational echo chemical exchange spectroscopy (CES) is meeting this challenge (1–7). 2D IR vibrational echo CES is akin to a 2D nuclear magnetic resonance (NMR) chemical exchange experiment (8), except that it can operate on picosecond timescales, and it directly probes the structural degrees of freedom through the time evolution of the 2D IR vibrational echo spectrum. Let us consider two molecular species that differ structurally (e.g., two distinct molecular structural isomers). A vibrational mode has a frequency that is different for the two species. The molecular vibrational oscillators of each subset are excited simultaneously by the first pulse in the 2D IR vibrational echo pulse sequence. The later pulses in the sequence generate observable signals that are sensitive to interconversion between species even if the aggregate populations of the two distinct species (the observable in linear spectroscopy) do not change. Ultrafast 2D IR vibrational echo CES makes it possible to directly measure the interconversion rate of chemical species under thermal equilibrium conditions.

This review describes the 2D IR vibrational echo pulse sequence (9–17) and discusses the specific application to CES. Three examples illustrate the method and provide important new insights into chemical and biological systems. The first example is solute-solvent complexes between phenols (2, 3, 18, 19) and silanols (20) as solutes with mixed solvents of benzenes and substituted benzenes and carbon tetrachloride. The alcohols form well-defined solute π-hydrogen-bonded complexes with the solvent. The hydroxyl stretch of the alcohol is monitored in the CES experiment. When complexed, the hydroxyl stretch has a different frequency than the uncomplexed (free) species.

The second example is rotational *gauche-trans* isomerization around a carbon-carbon single bond of a substituted ethane (4). During the course of isomerization, a molecule exchanges between relatively stable conformations by passing through unstable configurations. Rotational isomerization is a major factor in the dynamics, reactivity, and biological activity of a multiplicity of molecular structures. Techniques such as NMR can be applied only at low temperature to systems with very high barriers to slow the dynamics to the millisecond timescale (21). CES directly measures the isomerization time for a low barrier system at room temperature and permits a determination of the ethane isomerization time.

The final example is the dynamics of an elementary structural change in a protein. Proteins can fold into a number of well-defined structural substates. Under thermal equilibrium conditions, a protein undergoes transitions from one structural substate to another by passing over relatively low barriers. Proteins undergo large conformational changes on long timescales (milliseconds to seconds) such as those that occur following substrate binding to an enzyme. However, these slow transformations occur through a vast number of fast elementary conformational steps. CES was used to make the first measurement of the time for an elementary conformational step (7).

Two-dimensional infrared (2D IR) spectrum: an infrared spectrum with two frequency axes obtained from two Fourier transformations of time-dependent vibrational echo data

Vibrational echo: the infrared vibrational nonlinear spectroscopic equivalent of the NMR spin echo and the electronic excited-state photon echo

2D IR vibrational echo chemical exchange spectroscopy (CES): two-dimensional vibrational echo experiments that measure chemical exchange dynamics without perturbing the system's equilibrium

NMR: nuclear magnetic resonance

Solute-solvent complex: a weakly bound complex between a solute molecule and a solvent molecule that has a well-defined structure and lifetime

Structural substate: one of a number of well-defined structures of a folded protein that can be separated from other substates by relatively low barriers

2. THE ULTRAFAST 2D IR VIBRATIONAL ECHO CHEMICAL EXCHANGE SPECTROSCOPY METHOD

Details of the methods used for these 2D IR vibrational echo CES experiments have been described previously (3, 5, 22, 23). There are three excitation pulses, ~60 fs in duration produced with a Ti:sapphire regenerative amplifier pumped optical parametric amplifier. The optical parametric amplifier is tuned to the frequency of the vibrational mode under investigation. The IR pulses have sufficient bandwidth to span the spectral region of interest. The times between pulses 1 and 2 and between pulses 2 and 3 are referred to as τ and T_w, respectively. The vibrational echo signal radiates from the sample at a time $\leq\tau$ after the third pulse and is recorded by scanning τ at fixed T_w. The signal is spatially and temporally overlapped with a local oscillator for heterodyne detection, and the combined pulse is dispersed by a monochromator onto an IR array detector. Heterodyne detection provides both amplitude and phase information. Taking the spectrum of the heterodyne-detected vibrational echo signal performs one of the two Fourier transforms and gives the ω_m axis (where m indicates the axis obtained from the monochromator) in the 2D IR spectra. When τ is scanned, a temporal interferogram is obtained at each ω_m. The temporal interferograms are numerically Fourier transformed to give the other axis, the ω_τ axis. 2D IR spectra are obtained for a range of T_w's.

A 2D IR vibrational echo chemical exchange experiment works in the following manner. The first laser pulse labels the initial structures of the species by establishing their initial frequencies, ω_τ. The second pulse ends the first time period τ and starts the reaction time period T_w, during which the labeled species undergo chemical exchange (i.e., one type of species interconverts into the other). The third pulse ends the population period of length T_w and begins a third period of length $\leq\tau$, which ends with the emission of the vibrational echo pulse of frequency ω_m, which is the signal in the experiment. The vibrational echo signal reads out information about the final structures of all labeled species by their frequencies, ω_m. During the period T_w between pulses 2 and 3, chemical exchange occurs. The exchange causes new off-diagonal peaks to grow as T_w is increased. This growth is used to obtain the chemical exchange time constants.

Also needed for the data analysis are the vibrational population relaxation time constants and orientational relaxation time constants, which have been measured by polarization selective IR pump-probe experiments (3, 24). The enthalpies of formation of the solute-solvent complexes were determined from the temperature dependence of the equilibrium constants. The temperature-dependent equilibrium constants were obtained from the temperature dependence of the linear absorption spectra using Fourier transform infrared (FT-IR) spectroscopy (6, 18). Expression and purification of the mutant sperm whale myoglobin (Mb) L29I were performed as described previously (25). The CO forms of mutant Mb were prepared according to published protocols (26).

Heterodyne detection: combining the vibrational echo pulse with another pulse (local oscillator), produces interference that provides phase information and signal amplification

Chemical exchange: two species in equilibrium interconvert one to another without changing the steady-state quantities of the species

Off-diagonal peak: peak in a 2D IR vibrational echo spectrum that is above or below a diagonal peak

FT-IR: Fourier transform infrared

L29I: a mutant of myoglobin with leucine replaced by isoleucine at the twenty-ninth position

3. CHEMICAL EXCHANGE SPECTROSCOPY STUDIES OF STRUCTURAL DYNAMICS

3.1. Solute-Solvent Complexes

Solvents play an substantial role in practical chemistry by influencing the reactivity of dissolved substrates (27). Specific intermolecular interactions, such as hydrogen bonding, can lead to structurally characterizable solute-solvent complexes that are constantly forming and dissociating under thermal equilibrium conditions on very short timescales (28). The dynamics of these transient species can play an important role in the physical and chemical properties of a solute-solvent system by affecting reaction rates, reaction mechanisms, and product ratios (27). For the majority of

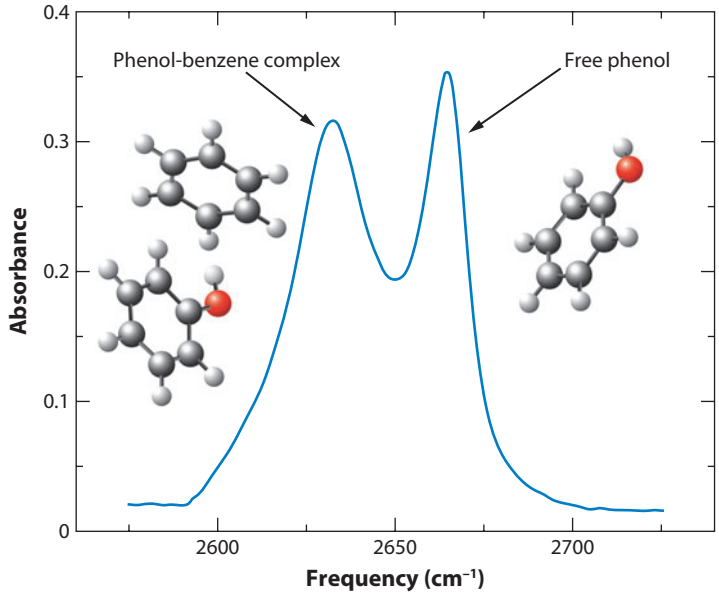

Figure 1

Absorption spectrum of the OD hydroxyl stretching mode of a phenol-benzene complex and free phenol (not a complex) in the mixed solvent of benzene and CCl_4. The molecular structures are also shown (2, 19).

organic and other types of nonaqueous solutions, the solute-solvent complexes form and dissociate on subnanosecond timescales (2, 18, 20), which cannot be measured by NMR and other methods.

Figure 1 shows the spectrum of the hydroxyl stretch of phenol-OD (OH hydroxyl replaced with OD) in the mixed solvent of benzene and CCl_4 (29 mol% benzene, 71 mol% CCl_4). Phenol-OD is used to shift the hydroxyl stretch absorption below the C-H stretch frequencies. The mixed solvent of benzene/CCl_4 shifts the equilibrium so that the two peaks are approximately the same amplitude. The spectrum shows that the two species coexist, but it does not yield information on the time dependence of the dissociation and formation of the complexes.

Figure 2*a* shows a 2D IR vibrational echo spectrum taken at a T_w that is short compared to the chemical exchange. The two bands on the diagonal arise from the two absorption peaks in **Figure 1**. The red bands are positive going and correspond to vibrational echo emission at the 0–1 vibrational transition frequency. The two blue bands (negative going) below the diagonal arise from vibrational echo emission at the 1–2 transition frequency. These peaks are shifted along the ω_m axis by the vibrational anharmonicity of the OD hydroxyl stretching potential. The ω_τ axis is the frequency of the first interaction with the radiation field (first pulse). The 0–1 peaks on the diagonal are produced as follows. The first pulse creates a 0–1 coherence (coherent superposition state), and the second pulse creates a population. There are two quantum pathways: In one, the population is created in the 1 level, and in the other the population is created in the 0 level. In either case, the third pulse again creates a 0–1 coherence, which subsequently gives rise to the vibrational echo at the frequency ω_m. Because the first interaction (ω_τ axis) and the vibrational echo emission (ω_m axis) are at the same frequency, the peaks are on the diagonal. The 1–2 off-diagonal peaks arise through a third quantum pathway. Again, the first pulse creates a 0–1 coherence, and the second pulse creates a population. For the pathway that creates the population in the 1 state, the third pulse can create a coherence between the 1–2 states, which produces the vibrational echo at the 1–2 transition frequency. The result is that the ω_τ position is the 0–1 frequency, but

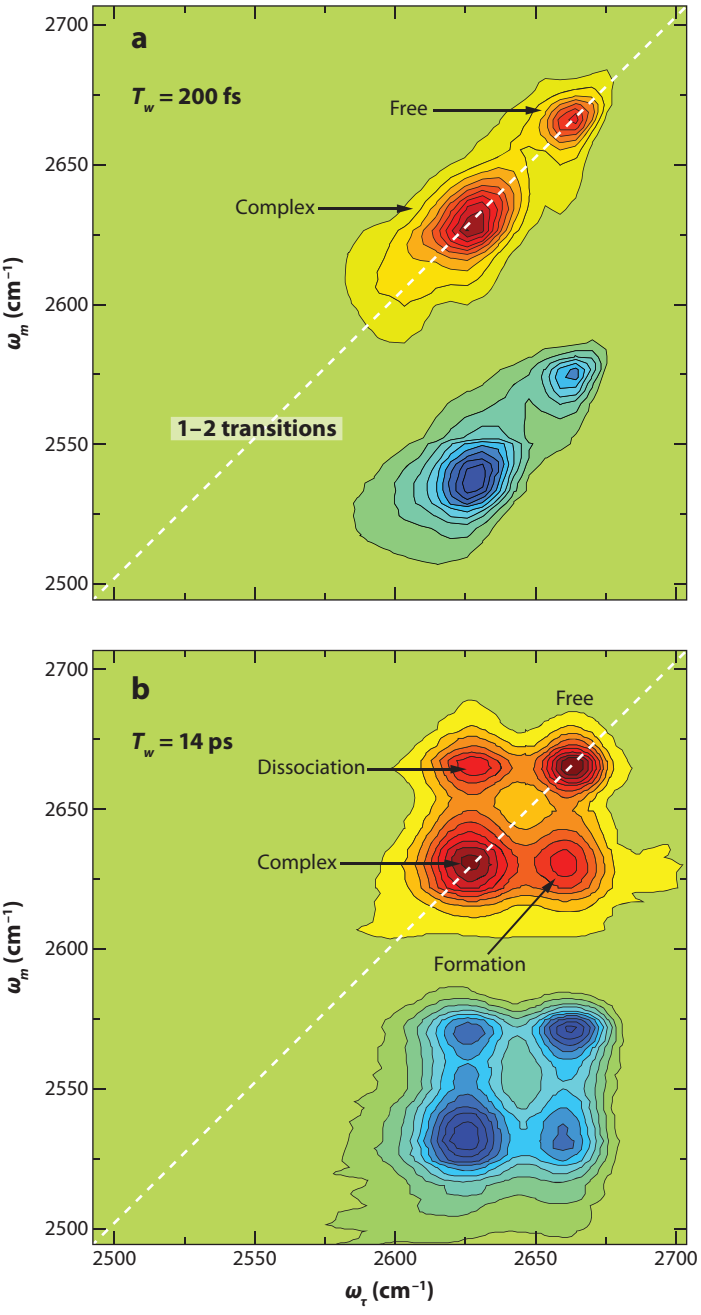

Figure 2

Two-dimensional infrared vibrational echo spectra of a phenol-benzene complex and free phenol. (*a*) The spectrum at short time prior to chemical exchange: peaks on the white dashed diagonal, positive going (*red*), 0–1 vibrational transitions, and peaks below the diagonal, negative going (*blue*), arising from emission at the 1–2 transition frequency. The blue peaks are shifted along the ω_m axis by the vibrational anharmonicity. (*b*) The spectrum at a time sufficiently long for considerable chemical exchange to have occurred. Complexes have dissociated, and free phenols have associated to form complexes producing the off-diagonal peaks in the 0–1 region (*red*) and the additional peaks in the 1–2 region (*blue*).

the ω_m position is the 1–2 frequency. Therefore, the bands are off-diagonal and shifted by the anharmonicity.

Diagonal peaks: peaks on the upper right to lower left diagonal in a 2D IR vibrational echo spectrum corresponding to absorption spectrum peaks

Peak volume: measure of a 2D IR vibrational echo spectral peak determined by amplitude and area and not affected by spectral diffusion

Figure 2*b* shows the 2D IR spectrum at a time that is sufficiently long for a substantial amount of chemical exchange to have occurred. Off-diagonal peaks have grown in. Let us consider the peak labeled dissociation in the 0–1 portion of the spectrum. At the time of the first pulse, species that are complexes have a frequency $\omega_\tau = 2630\ \text{cm}^{-1}$. Complexes that dissociate during the interval $T_w = 14$ ps become free and give rise to vibrational echo emission at a frequency $\omega_m = 2665\ \text{cm}^{-1}$. Therefore, the peak is off-diagonal and to the upper left of the diagonal, corresponding to dissociation. The peak corresponding to formation arises in the same manner. Free species form complexes and give rise to the other off-diagonal peak. The peaks on the diagonal correspond to species that have not changed their character. Importantly, the time-dependent growth of the off-diagonal peaks yields direct information on the rate of chemical exchange.

Figure 3 shows 3D representations of the 0–1 region of the 2D IR spectrum for several T_w's. As T_w increases, the off-diagonal peaks grow in. The chemical exchange time clearly is greater than 1 ps and is on the order of a number of picoseconds. To analyze the data in detail, one must take into account the other dynamics that influence 2D IR vibrational echo CES (2, 5). The vibrational excited states decay to the ground state with lifetimes T_1. The free and complex species undergo orientational relaxation, with orientational relaxation time constants τ_r. The T_1's cause all the peaks to decay to zero, whereas the τ_r's cause all the peaks to be reduced in amplitude, but not to decay to zero. The chemical exchange causes the diagonal peaks to decay and the off-diagonal peaks to grow. Another contribution is spectral diffusion, which is caused by thermal fluctuations that produce fluctuations in the transition frequency of a species (29–34). Spectral diffusion changes the shape and amplitude of the peaks, but it does not change the peak volumes (2, 5).

In fitting the data, one can measure independently all the necessary input parameters except for the chemical exchange rate. The T_1's and τ_r's are measured with IR polarization and wavelength-selective pump-probe spectroscopy. The time-dependent peak volumes are used rather than the peak amplitudes to eliminate the contribution from spectral diffusion (2, 5). In addition, it is necessary to know the equilibrium constant and the ratio of the complex and free OD stretch transition dipoles, which are obtained with IR absorption spectroscopy (2, 18). Therefore, the time dependence the CES data can be fit with a single adjustable parameter, the complex dissociation time, τ_d, which is the inverse of the dissociation rate constant. The single parameter τ_d can be used because the system is in equilibrium (2), and therefore, the rate of formation is equal to the rate of dissociation.

Figure 4 shows the results of fitting the CES data for phenol-OD in the mixed benzene-CCl_4 solvent. The T_w dependent data in **Figure 4** are for the 0–1 portion of the 2D IR spectra. There are four peaks, two diagonal and two off-diagonal. Because the system's thermal equilibrium is not perturbed by the excitation of the hydroxyl stretch (2), the off-diagonal peaks grow in at the same rate. The curves through the data points are obtained from the fit using the single adjustable parameter, τ_d. Clearly, the fit is very good and yields the phenol-benzene complex dissociation time, $\tau_d = 10$ ps (2, 18).

Thirteen solute-solvent complexes have been studied with 2D IR vibrational echo CES. Eight of them have phenol or substituted phenols as the solutes (18) and the other five have triethylsilanol-OD as the solute (20). All have solvents of substituted benzenes–CCl_4 mixed solvents except for one that is triethylsilanol-OD in acetonitrile-CCl_4. The enthalpies of formation of the complexes, ΔH^0, range from -0.6 kcal mol^{-1} to -3.3 kcal mol^{-1}. **Figure 5** shows data for five of the phenol systems at the same waiting time, $T_w = 7$ ps. From left to right, ΔH^0 becomes smaller and τ_d becomes shorter. This is evident by the size of the off-diagonal peaks. For mesitylene (three

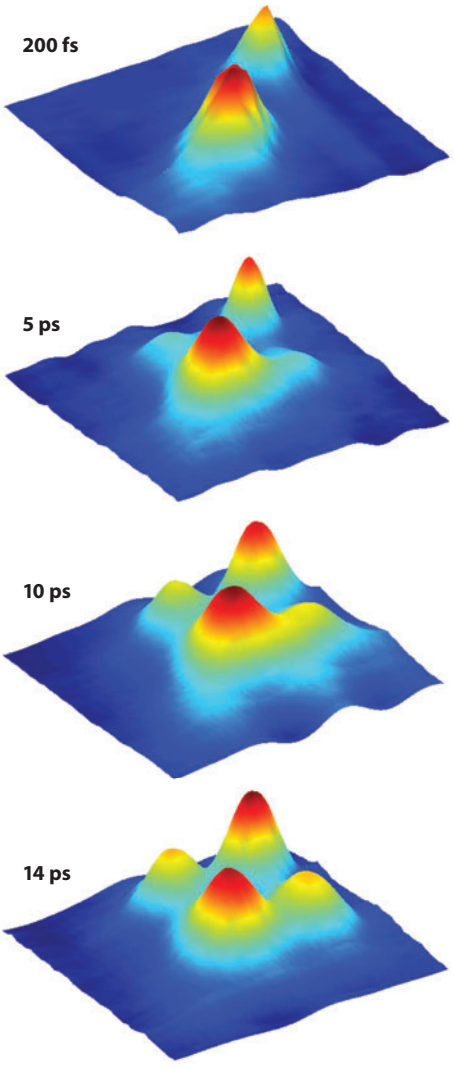

Figure 3

Three-dimensional representation of the growth of the off-diagonal peaks in the 0–1 spectral region owing to chemical exchange. As time increases, the off-diagonal peaks grow in.

methyls donating electron density to the ring, making the π hydrogen bond stronger), the off-diagonal peaks are just beginning to appear at 7 ps. For toluene (one methyl), the off-diagonal peaks are well developed at 7 ps. For bromobenzene (the bromo is electron withdrawing, making the π hydrogen bond weak), the off-diagonal peaks are so large at 7 ps that they have merged with the diagonal peaks to give a square shape.

Figure 6 displays the dissociation times, $\tau_d = 1/k_d$, for the 13 complexes (18, 20). The data are plotted versus $\exp(-\Delta H^0/RT)$, where ΔH^0 is the enthalpy of formation of the complexes. Over a range of dissociation times from ~4 ps to ~140 ps and ΔH^0 values ranging from -0.6 kcal mol^{-1} to -3.3 kcal mol^{-1}, the experimental points fall on a line. Transition-state theory

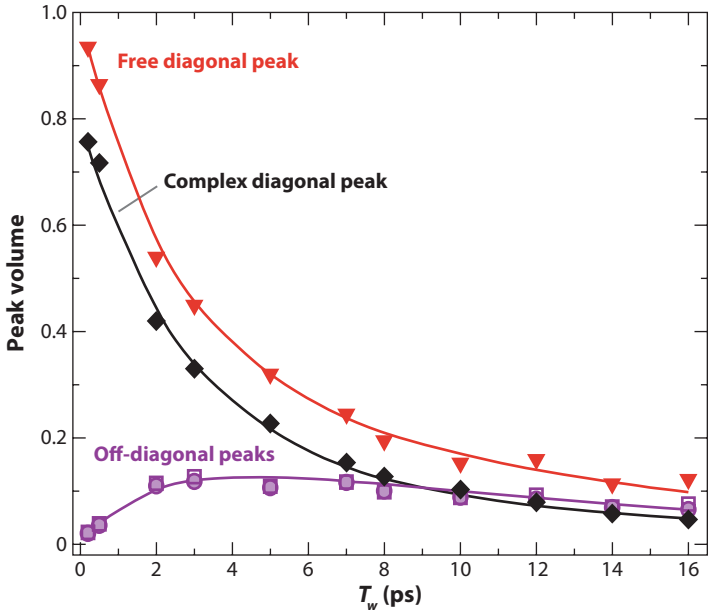

Figure 4

Data points (*symbols*) for the diagonal and off-diagonal peaks as a function of the time, T_w. The solid lines through the data are the result of a fit with a single adjustable parameter, τ_d.

(35) states that k_d depends on the activation free energy, ΔG^*, not on the enthalpy of formation, ΔH^0. However, if the activation enthalpy is proportional to the dissociation enthalpy, $\Delta H^* \propto \Delta H^0$, and the activation entropy ΔS^* is essentially a constant, then the behavior displayed in **Figure 6** is obtained. The results shown in **Figure 6** indicate that the enthalpy of formation of a solute-solvent complex can be used as a guide for its dissociation time.

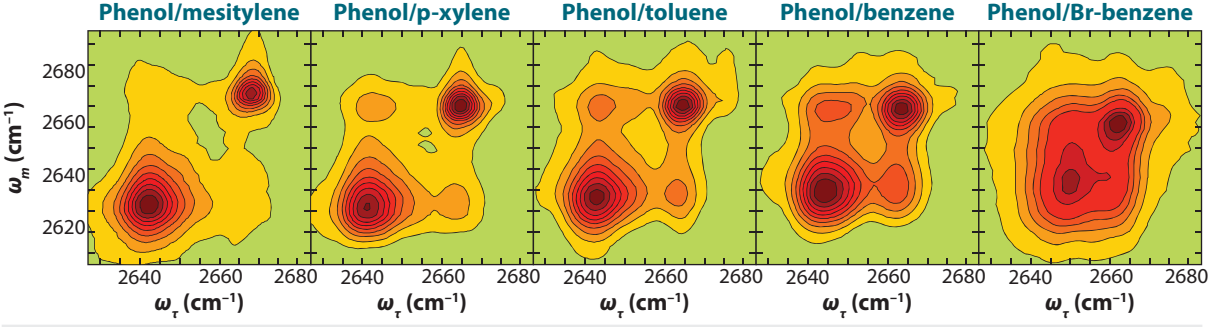

ΔH^0 (kcal mol^{-1})	−2.45	−2.23	−1.98	−1.67	−1.21
τ_d (ps)	32	24	15	10	5

Figure 5

Data at a single time, $T_w = 7$ ps, for five phenol complexes with substituted benzenes. The enthalpies of formation (ΔH^0) and the dissociation times (τ_d) are given for each complex below the corresponding 2D spectrum.

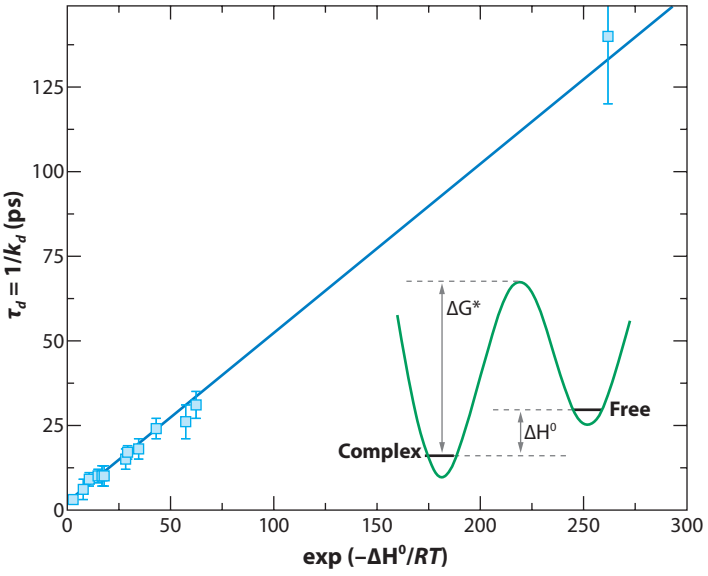

Figure 6

A plot of the dissociation times, τ_d, of 13 complexes versus $\exp(-\Delta H^0/RT)$. The points fall on a line, showing the dissociation time is related to the ΔH^0's. ΔG^* is the activation free energy.

3.2. Orientational Isomerization About a Carbon-Carbon Single Bond

Ethane and its derivatives are textbook examples of molecules that undergo orientational isomerization around a carbon-carbon single bond (36). In ethane, the transition from one staggered state to another leaves ethane structurally identical. Therefore, CES cannot be performed on ethane because there is no change in vibrational frequency with the isomerization. In contrast, a 1,2-di-substituted ethane has two distinct staggered conformations, *gauche* and *trans*, that have distinguishing characteristics because of the relative positions of the two substituents (36).

The *trans-gauche* isomerization of 1,2-di-substituted ethane derivatives (e.g., *n*-butane) is one of the simplest cases of a first-order chemical reaction. This type of isomerization has served as a basic model for modern chemical reaction kinetic theory and molecular dynamics (MD) simulation studies in condensed phases (37–42). Despite extensive theoretical investigation, until recently no corresponding kinetic experiments had been performed to test the results (4). The experimental difficulty resulted from the low rotational energy barrier of the *n*-butane (~3.3 kcal mol^{-1}) and other simple 1,2-di-substituted ethane derivatives (43). According to theoretical studies (37–42), the isomerization timescale ($1/k$, where k is the rate constant) is in the range of 10 to 100 ps in room-temperature liquids.

Ultrafast 2D IR vibrational echo CES was used to measure the *gauche-trans* isomerization about the carbon-carbon single bond of 1-fluoro-2-isocyanato-ethane (FICE) (4). FICE was studied in CCl_4 at room temperature, and the isocyanate group (N=C=O) was used as the vibrational probe. **Figure 7** shows the structure of FICE in the *gauche* and *trans* conformations and the spectrum of the isocyanate antisymmetric stretching mode in the two conformations. The *gauche* and *trans* structures and their assignment to the peaks in the spectrum were obtained from electronic structure calculations using density functional theory (44) at the B3LYP level and 6–31+ G(d,p) basis set for the isolated molecules. The calculation also gave the barrier height for the eclipsed transition state as 3.3 kcal mol^{-1} (4).

MD: molecular dynamics

FICE: 1-fluoro-2-isocyanato-ethane

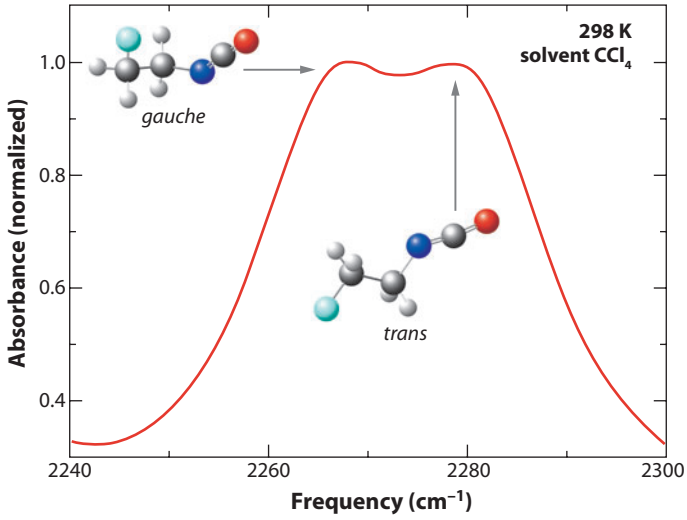

Figure 7

Absorption spectrum of the antisymmetric stretch of the isocyanate group of 1-fluoro-2-isocyanato-ethane. The two peaks arise from the *gauche* and *trans* isomers. The *gauche* and *trans* molecular structures obtained from electronic structure calculations are also shown.

In addition to the two peaks shown in **Figure 7**, there is another smaller unassigned combination band or overtone absorption at 2230 cm^{-1} (4). This small peak is coupled by anharmonic terms in the molecular potential to the antisymmetric isocyanate stretching mode. The coupling produces additional off-diagonal peaks in the spectrum (4, 45). The nature of these additional off-diagonal peaks was investigated in detail by observing the 2D IR vibrational echo spectra of 1-bromo-2-isocyanato-ethane (4). The bromo group is so bulky that it raises the barrier height to the point at which no *gauche-trans* isomerization occurs on the experimental timescale of ~50 ps. The results of the experiments on the bromo compound show that there is a negative-going off-diagonal band that overlaps the off-diagonal position at which one of the positive-going chemical exchange peaks will grow in owing to isomerization in the fluoro compound. The presence of this additional negative-going peak is included in the data analysis.

Figure 8*a* shows 2D IR spectra of FICE in a CCl_4 solution at room temperature taken at four T_w's. The 200-fs panel corresponds to a short T_w at which negligible isomerization has occurred. The two peaks representing the *gauche* ($\omega_m = 2265\ cm^{-1}$) and *trans* ($\omega_m = 2280\ cm^{-1}$) conformers are on the diagonal. For a long time ($T_w = 25$ ps), isomerization has proceeded to a substantial degree. The obvious change is the additional peak appearing in the upper left ($\omega_\tau = 2265\ cm^{-1}$ and $\omega_m = 2280\ cm^{-1}$), which arises from the *gauche*-to-*trans* isomerization. There is a corresponding peak to the lower right that is generated by the *trans*-to-*gauche* isomerization, but it is reduced in amplitude by the negative-going peak discussed briefly above (4, 45). **Figure 8*b*** presents calculated spectra that include the isomerization kinetics, the other off-diagonal peaks, and the vibrational dynamics other than the isomerization. Although the system is more complicated than the solute-solvent complex chemical exchange, the data can be reproduced well by the calculations (4).

Figure 9 shows the T_w-dependent data for the diagonal and off-diagonal peaks. As in the solute-solvent complex experiments, all the necessary input parameters are known except for the isomerization time, $\tau_{iso} = 1/k_{GT} = 1/k_{TG}$ (4). In the analysis, the *gauche*-to-*trans* rate constant was taken to be equal to the *trans*-to-*gauche* rate constant. Within experimental error, the difference in the two rate constants could not be discerned. The solid curves through the data are the result

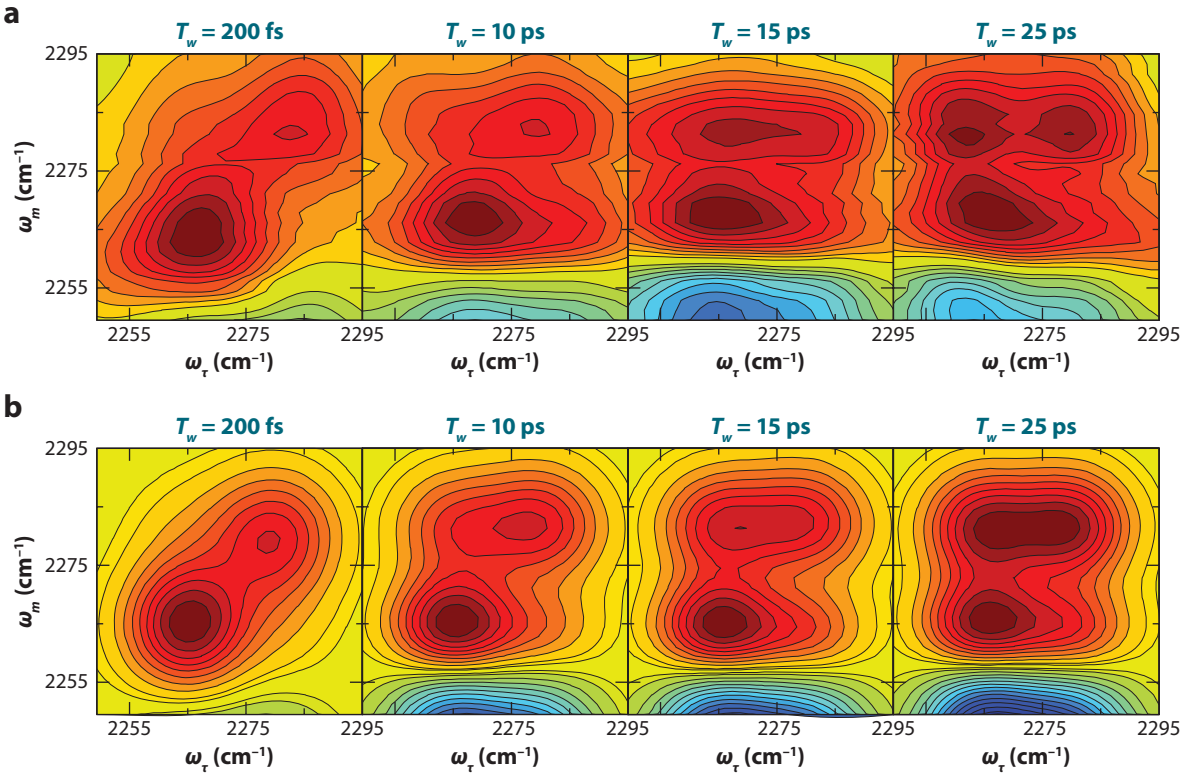

Figure 8

(*a*) Two-dimensional infrared vibrational echo chemical exchange spectroscopy data, showing the *gauche-trans* isomerization of 1-fluoro-2-isocyanato-ethane around the carbon-carbon single bond in the 0–1 spectral region. By 25 ps, the upper left off-diagonal chemical exchange peak is substantial. The corresponding peak to the lower right is less pronounced because of overlap with a negative-going peak. (*b*) Model calculations including all dynamics that influence the 2D IR spectrum.

of the fit with the single adjustable parameter, τ_{iso}. The isomerization time is $\tau_{iso} = 43 \pm 10$ ps. The error bars arise from the uncertainty in the parameters that go into the calculations.

Based on the experimental results for FICE, the *gauche-trans* isomerization rate of *n*-butane and the rotational isomerization rate of ethane under the same conditions used in this study (CCl_4 solution at room temperature, 297 K) were calculated approximately using transition-state theory (46). The prefactors were taken to be the same because the transition states and the barrier heights are quite similar for the three systems (4). The barrier heights were calculated using density functional theory on all the systems through the same method [the B3LYP level and 6–31+ G(d,p) basis set]. With the zero-point energy correction, the *trans*-to-*gauche* isomerization of *n*-butane has a barrier of 3.3 kcal mol^{-1}. The barrier for ethane was calculated to be 2.5 kcal mol^{-1} (4), which is smaller than the result of more extensive calculations, 2.9 kcal mol^{-1} (47, 48). The 2.5 kcal mol^{-1} value was used for ethane so that all the barriers were obtained with the same method, which should result in some cancellation of errors.

The use of the calculated barriers for FICE and for *n*-butane gave a ~40 ps time constant for the *n*-butane *trans*-to-*gauche* isomerization time constant ($1/k_{TG}$). Rosenberg, Berne, and Chandler (40) reported a 43-ps time constant for this process (in CCl_4 at 300 K) from MD simulations. Other MD simulations gave isomerization rates in liquid *n*-butane at slightly lower temperatures:

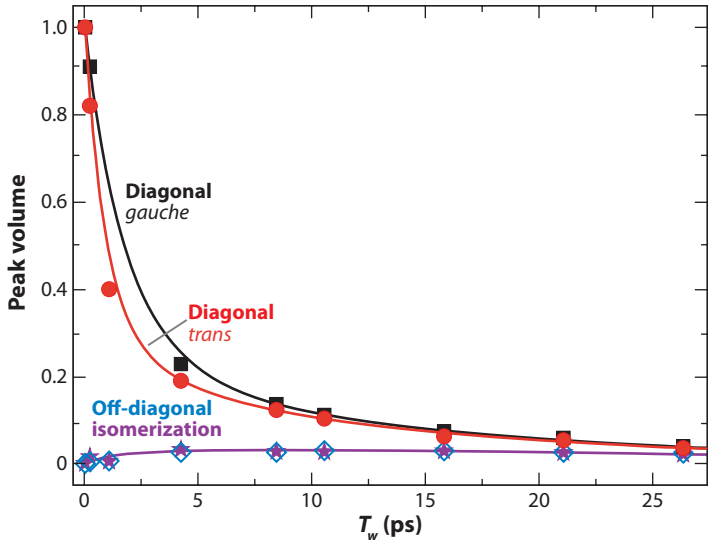

Figure 9

The diagonal and off-diagonal two-dimensional infrared vibrational echo chemical exchange spectroscopy data for the *gauche-trans* isomerization of 1-fluoro-2-isocyanato-ethane around the carbon-carbon single bond (*symbols*) and the single adjustable parameter fit (*solid curves*).

52 ps (292 K) (41), 57 ps (292 K) (39), 50 ps (273 K) (39), and 61 ps (<292 K) (42). All these values are quite close to the value based on the experimental measurements on FICE. In the same manner, the isomerization time constant for ethane is found to be ~12 ps. This value can be improved by better electronic structure calculations on FICE and calculations for both FICE and ethane that include CCl_4 in determining the barriers. Thus, this first experimental determination of the time constant for the orientational isomerization about a carbon-carbon single bond for a di-substituted ethane with a low barrier in solution at room temperature also provides the first experimentally based value for the ethane isomerization time constant.

3.3. Fast Protein Conformational Switching

A folded protein with a particular structure occupies a minimum on its free energy landscape (49–51). Other minima of similar energy can also exist. The different conformational structures associated with these minima are substates of the folded protein. The ability of proteins to undergo conformational switching between substates is central to their function. Proteins can undergo large conformational changes, which occur on long timescales (milliseconds to seconds). However, these large slow conformational changes—such as those that occur following substrate binding by an enzyme (52) or protein folding (53)—involve a large number of elementary conformational steps. The experimental determination of the rates of elementary conformational steps is a long-standing problem that has now been successfully addressed using ultrafast 2D IR vibrational echo CES (7).

Conformational switching: the interconversion from one protein substate to another

MbCO: the protein myoglobin with carbon monoxide bound at the active site

The problem of multiple substates has been studied extensively for the protein Mb with the ligand CO bound at the active site (MbCO) (54–56). The IR spectrum of the heme-ligated CO stretching mode of Mb has three absorption bands: A_0 (1965 cm^{-1}), A_1 (1945 cm^{-1}), and A_3 (1932 cm^{-1}) (57). MbCO interconverts among these three conformational substates under thermal equilibrium conditions. The distal histidine His64 plays a prominent role in determining the conformational substates of Mb. Here a study of an Mb mutant, L29I (leucine replaced

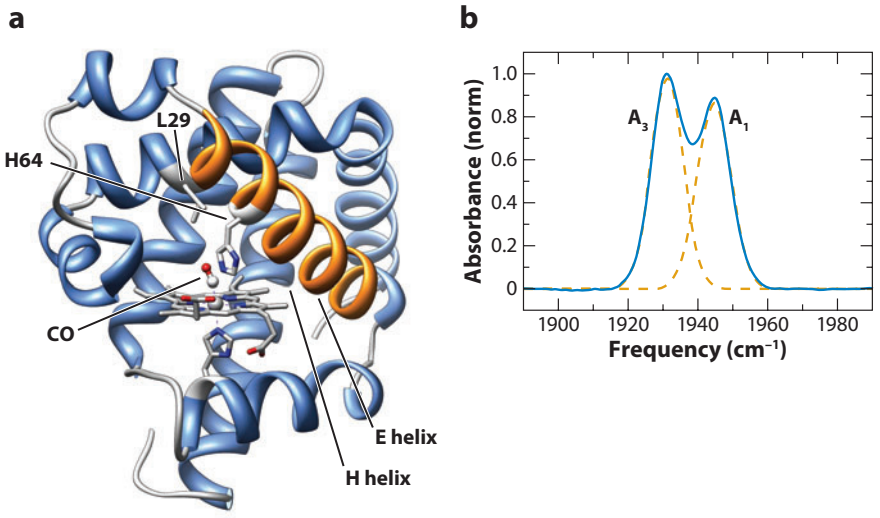

Figure 10

(*a*) Structure of the myoglobin mutant L29I (leucine replaced by isoleucine) with CO bound at the active site. A_1–A_3 structural substate switching causes the E helix to shift and the imidazole side group of H64 to change conformation. (*b*) Background subtracted infrared absorption spectrum of the CO stretch of CO bound to L29I. The two structural substates give rise to the two absorption bands.

by an isoleucine), is presented (see **Figure 10*a***). This small change makes the A_1 and A_3 CO bands almost equal in amplitude (**Figure 10*b***). Changes in the configuration of the E helix (see **Figure 10*a***) cause the distal histidine's imidazole side group to move relative to the CO (57, 58). With H64's imidazole in the heme pocket, the lower frequency of A_3 compared with A_1 reflects the closer proximity of the imidazole to the CO in A_3 (26, 58, 59). Each A substate exhibits a distinct ligand-binding rate (50, 54). Therefore, the peaks in the FT-IR spectrum of MbCO reflect functionally distinct conformational substates.

Figure 11 displays 2D-IR spectra of CO bound to L29I at several T_w's. The red bands are positive going and correspond to the 0–1 vibrational transitions. The blue bands (negative going) are from the 1–2 transition. For $T_w = 0.5$ ps, only the two diagonal peaks are observed. These correspond to the A_1 and A_3 bands in the FT-IR spectrum shown in **Figure 10*b***. As T_w increases, the off-diagonal chemical exchange peaks grow in. By $T_w = 48$ ps, the off-diagonal bands are readily apparent. The band to the upper left in the $T_w = 48$ ps panel is strong. Because the anharmonicity is not large, the negative-going 1–2 band partially overlaps the positive-going off-diagonal chemical exchange peak to the lower right of the two 0–1 diagonal peaks, reducing its amplitude.

In the data analysis, the peak volumes were fit, and both the positive (0–1) and negative (1–2) peaks were included (7). Only the vibrational lifetimes were included in the kinetic data analysis because the orientational relaxation of the protein is very slow. The experimental diagonal and off-diagonal peak volumes for the 0–1 region of the spectra are plotted in **Figure 12**. The solid lines through the data points are obtained from the fitting procedure with the substate switching time, τ_{13}, as the single adjustable parameter. The results of the fitting yield $\tau_{13} = 47$ ps $\pm$ 8 ps. Within experimental error, $\tau_{13} = \tau_{31}$.

X-ray experiments demonstrate that significant structural change occurs in the A_1–A_3 interconversion. The high-resolution crystal structure of MbCO that contains two conformations has enabled modeling of the structure of A_1 and A_3 substates (58, 60). Structural comparison of the A_1

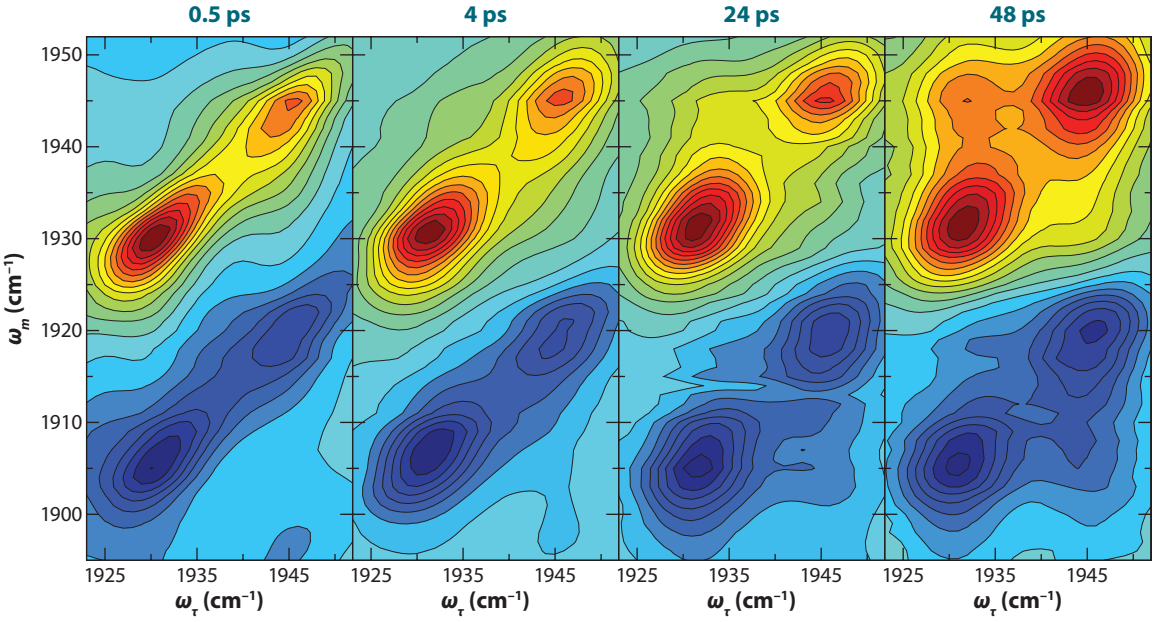

Figure 11

Two-dimensional infrared vibrational echo chemical exchange spectroscopy data showing A_1–A_3 protein structural substate switching. By 48 ps, the upper left off-diagonal chemical exchange peak is substantial. The corresponding off-diagonal peak in the 0–1 transition region (*red*) to the lower right of the diagonal is less pronounced because of overlap with the negative-going 1–2 transition region peak (*blue*).

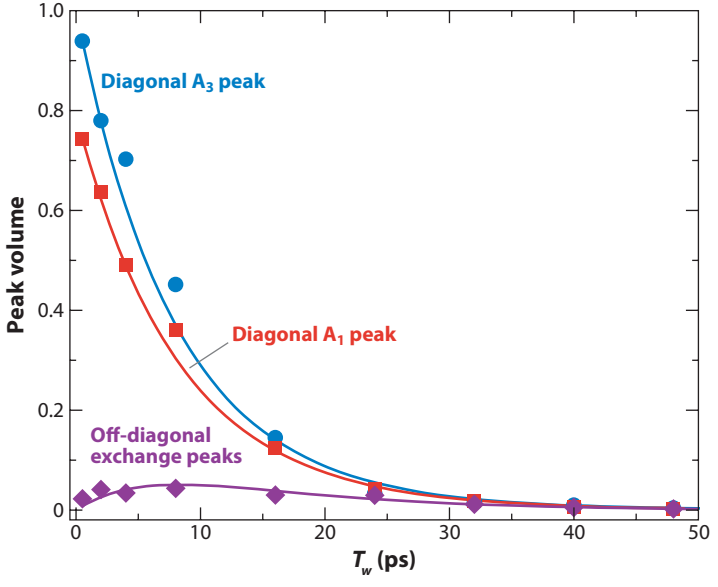

Figure 12

The diagonal and off-diagonal two-dimensional infrared vibrational echo chemical exchange spectroscopy data for the A_1–A_3 protein structural substate switching (*symbols*) and the single adjustable parameter fit (*solid curves*). The fit yields the substate switching time, 47 ps.

and A_3 substates shows that the A_3 substate contains an additional xenon cavity, Xe3, and another transient cavity found in simulations (60). Xe is used as a probe to identify the locations of cavities in proteins (61, 62). In Mb crystals, four Xe atoms (Xe1, Xe2, Xe3, and Xe4) occupy cavities, which may be involved in gas ligand migration (60, 61). The Xe3 site, which is near the surface and far from the iron atom, involves Trp7 and is located between helices E and H (61) (see **Figure 10*a***). That Xe3 exists in the A3 substate but not in the A1 substate demonstrates that the structural differences in the substates are long range and significant.

4. CONCLUDING REMARKS

This review describes ultrafast 2D IR vibrational echo CES and gives three examples: solute-solvent complex dynamics, isomerization, and protein conformational switching. This method measures dynamics in the ground electronic state under thermal equilibrium conditions, and it can be applied to a wide variety of problems. However, there are three conditions necessary to apply the technique: (*a*) There must be at least one IR-active mode that has a distinct frequency for each species undergoing exchange; (*b*) the concentrations of the species must be high enough for detection; and (*c*) the exchange rate must fall within the experimental window set by the lifetime of the vibration used as the probe. The vibrational mode used as the probe need not be directly involved in the exchange process. It is sufficient that the exchange causes the mode frequency to change.

SUMMARY POINTS

1. Ultrafast 2D IR vibrational echo CES can measure the dynamics of fast chemical processes under thermal equilibrium conditions without perturbing the systems dynamics.
2. The 2D IR vibrational echo pulse sequence uses a vibrational mode to label chemical species that are interconverting one to another. The interconversion does not change the overall number of each species, yet it is manifested in the growth of off-diagonal peaks in the 2D spectrum.
3. The growth rate of the off-diagonal peaks in a 2D IR vibrational echo CES permits the direct determination of the interconversion rates between species. In each presented example, the only adjustable parameter necessary to fit the data was the chemical exchange rate.
4. The formation and dissociation kinetics of 13 organic solute-solvent complexes have been studied. The dissociation times of the complexes ranged from 4 ps to 140 ps, and these times were correlated to the enthalpies of formation of the complexes, which ranged from -0.6 kcal mol^{-1} to -3.3 kcal mol^{-1}.
5. The rate of rotational isomerization around a carbon-carbon single bond in liquid solution at room temperature for a di-substituted ethane with a low barrier was measured for the first time. The experimental result confirmed the accuracy of simulations of closely related systems.
6. Using the experimental isomerization time for the di-substituted ethane, it was found that the isomerization time for ethane is approximately 12 ps.
7. The long-standing problem of the rate of structural substate interconversion for the protein MbCO has been solved. The time for this single elementary structural interconversion between the A_1 and A_3 substates was found to be 47 ps.

8. The applications of ultrafast 2D IR vibrational echo CES are expanding rapidly. The method will prove useful in a wide variety of fields and will become increasingly accessible as the technology and methodology continue to improve.

DISCLOSURE STATEMENT

The author is not aware of any biases that might be perceived as affecting the objectivity of this review.

ACKNOWLEDGMENTS

I would like to thank Junrong Zheng, who was primarily responsible for the solute-solvent complex experiments with considerable help from coworkers. Kyungwon Kwak contributed to the solute-solvent complex experiments and did a great deal of associated theoretical work. Junrong Zheng was responsible for the isomerization experiments. Haruto Ishikawa was primarily responsible for the protein substate switching experiments, with theoretical and experimental help from Kyungwon Kwak, Jean K. Chung, and Seongheun Kim. I would also like to thank the Air Force Office of Scientific Research (F49620-01-1-0018), the National Science Foundation (DMR 0652232), and the National Institutes of Health (2 R01 GM-061137-05) for support of this work.

LITERATURE CITED

1. Kim YS, Hochstrasser RM. 2005. Chemical exchange 2D IR of hydrogen-bond making and breaking. *Proc. Natl. Acad. Sci. USA* 102:11185–90
2. Zheng J, Kwak K, Asbury JB, Chen X, Piletic I, Fayer MD. 2005. Ultrafast dynamics of solute-solvent complexation observed at thermal equilibrium in real time. *Science* 309:1338–43
3. Zheng J, Kwak K, Chen X, Asbury JB, Fayer MD. 2006. Formation and dissociation of intra-intermolecular hydrogen bonded solute-solvent complexes: chemical exchange 2D IR vibrational echo spectroscopy. *J. Am. Chem. Soc.* 128:2977–87
4. Zheng J, Kwac K, Xie J, Fayer MD. 2006. Ultrafast carbon-carbon single bond rotational isomerization in room temperature solution. *Science* 313:1951–55
5. Kwak K, Zheng J, Cang H, Fayer MD. 2006. Ultrafast 2D IR vibrational echo chemical exchange experiments and theory. *J. Phys. Chem. B* 110:19998–20013
6. Zheng J, Kwak K, Fayer MD. 2007. Ultrafast 2D IR vibrational echo spectroscopy. *Acc. Chem. Res.* 40:75–83
7. Ishikawa H, Kwak K, Chung JK, Kim S, Fayer MD. 2008. Direct observation of fast protein conformational switching. *Proc. Natl. Acad. Sci. USA* 105:8619–24
8. Jeener J, Meier BH, Bachmann P, Ernst RR. 1979. Investigation of exchange processes by two-dimensional NMR spectroscopy. *J. Chem. Phys.* 71:4546–53
9. Asplund MC, Zanni MT, Hochstrasser RM. 2000. Two-dimensional infrared spectroscopy of peptides by phase-controlled femtosecond vibrational photon echoes. *Proc. Natl. Acad. Sci. USA* 97:8219–24
10. Khalil M, Demirdoven N, Tokmakoff A. 2003. Obtaining absorptive line shapes in two-dimensional infrared vibrational correlation spectra. *Phys. Rev. Lett.* 90:047401
11. Khalil M, Demirdoven N, Tokmakoff A. 2003. Coherent 2D IR spectroscopy: molecular structure and dynamics in solution. *J. Phys. Chem. A* 107:5258–79
12. Asbury JB, Steinel T, Stromberg C, Gaffney KJ, Piletic IR, et al. 2003. Hydrogen bond dynamics probed with ultrafast infrared heterodyne detected multidimensional vibrational stimulated echoes. *Phys. Rev. Lett.* 91:237402

13. Steinel T, Asbury JB, Corcelli SA, Lawrence CP, Skinner JL, Fayer MD. 2004. Water dynamics: dependence on local structure probed with vibrational echo correlation spectroscopy. *Chem. Phys. Lett.* 386:295–300
14. Mukherjee P, Kass I, Arkin I, Zanni MT. 2006. Picosecond dynamics of a membrane protein revealed by 2D IR. *Proc. Natl. Acad. Sci. USA* 103:3528–33
15. Maekawa H, Toniolo C, Moretto A, Broxterman QB, Ge NH. 2006. Different spectral signatures of octapeptide 3_{10}- and α-helices revealed by two-dimensional infrared spectroscopy. *J. Phys. Chem. B* 110:5834–37
16. Naraharisetty SRG, Kasyanenko VM, Rubtsov IV. 2008. Bond connectivity measured via relaxation-assisted two-dimensional infrared spectroscopy. *J. Chem. Phys.* 128:104502
17. Nee MJ, McCanne R, Kubarych KJ, Joffre M. 2007. Two-dimensional infrared spectroscopy detected by chirped pulse upconversion. *Opt. Lett.* 32:713–15
18. Zheng J, Fayer MD. 2007. Hydrogen bond lifetimes and energetics for solute-solvent complexes studied with 2D-IR vibrational echo spectroscopy. *J. Am. Chem. Soc.* 129:4328–35
19. Kwac K, Lee C, Jung Y, Han J, Kwak K, et al. 2006. Phenol-benzene complexation dynamics: quantum chemistry calculation, MD simulations, and 2D IR spectroscopy. *J. Chem. Phys.* 125:244508
20. Zheng J, Fayer MD. 2008. Solute-solvent complex kinetics and thermodynamics probe by 2D-IR vibrational echo chemical exchange spectroscopy. *J. Phys. Chem. B* 112:10221–27
21. Jackman LM, Cotton FA. 1975. *Dynamic Nuclear Magnetic Resonance Spectroscopy*. New York: Academic
22. Asbury JB, Steinel T, Fayer MD. 2004. Vibrational echo correlation spectroscopy probes hydrogen bond dynamics in water and methanol. *J. Lumin.* 107:271–86
23. Park S, Kwak K, Fayer MD. 2007. Ultrafast 2D-IR vibrational echo spectroscopy: a probe of molecular dynamics. *Laser Phys. Lett.* 4:704–18
24. Tan H-S, Piletic IR, Fayer MD. 2005. Orientational dynamics of nanoscopic water in reverse micelles: ultrafast infrared frequency selective transient absorption experiments. *J. Chem. Phys.* 122:174501
25. Varadarajan R, Szabo A, Boxer SG. 1985. Cloning, expression in *Escherichia coli*, and reconstitution of human myoglobin. *Proc. Natl. Acad. Sci. USA* 82:5681–84
26. Merchant KA, Noid WG, Akiyama R, Finkelstein I, Goun A, et al. 2003. Myoglobin-CO substate structures and dynamics: multidimensional vibrational echoes and molecular dynamics simulations. *J. Am. Chem. Soc.* 125:13804–18
27. Reichardt C. 2003. *Solvents and Solvent Effects in Organic Chemistry*. Weinheim: Wiley-VCH
28. Vinogradov SN, Linnell RH. 1971. *Hydrogen Bonding*. New York: Van Nostrand Reinhold Co.
29. Mukamel S. 2000. Multidimensional femtosecond correlation spectroscopies of electronic and vibrational excitations. *Annu. Rev. Phys. Chem.* 51:691–729
30. Mukamel S. 1995. *Principles of Nonlinear Optical Spectroscopy*. New York: Oxford Univ. Press
31. Asbury JB, Steinel T, Stromberg C, Corcelli SA, Lawrence CP, et al. 2004. Water dynamics: vibrational echo correlation spectroscopy and comparison to molecular dynamics simulations. *J. Phys. Chem. A* 108:1107–19
32. Asbury JB, Steinel T, Kwak K, Corcelli S, Lawrence CP, et al. 2004. Dynamics of water probed with vibrational echo correlation spectroscopy. *J. Chem. Phys.* 121:12431–46
33. Kwak K, Rosenfeld DE, Fayer MD. 2008. Taking apart 2D-IR vibrational echo spectra: more information and elimination of distortions. *J. Chem. Phys.* 128:204505
34. Kwak K, Park S, Finkelstein IJ, Fayer MD. 2007. Frequency-frequency correlation functions and apodization in 2D-IR vibrational echo spectroscopy, a new approach. *J. Chem. Phys.* 127:124503
35. Chang R. 2000. *Physical Chemistry for the Chemical and Biological Sciences*. Sausalito, Calif.: Univ. Sci. Books. 1018 pp.
36. March J. 1985. *Advanced Organic Chemistry*. New York: Wiley & Sons. 1346 pp.
37. Chandler D. 1978. Statistical mechanics of isomerization dynamics in liquids and the transition state approximation. *J. Chem. Phys.* 68:2959–70
38. Weber TA. 1978. Simulation of *n*-butane using a skeletal alkane model. *J. Chem. Phys.* 69:2347–54
39. Brown D, Clarke JHR. 1990. A direct method of studying reaction rates by equilibrium molecular dynamics: application to the kinetics of isomerization in liquid *n*-butane. *J. Chem. Phys.* 92:3062–73

40. Rosenberg RO, Berne BJ, Chandler D. 1980. Isomerization dynamics in liquids by molecular dynamics. *Chem. Phys. Lett.* 75:162–68
41. Edberg R, Evans DJ, Morris GP. 1987. Conformational kinetics in liquid butane by nonequilibrium molecular dynamics. *J. Chem. Phys.* 87:5700–8
42. Ramirez J, Laso M. 2001. Conformational kinetics in liquid *n*-butane by transition path sampling. *J. Chem. Phys.* 115:7285–92
43. Streitwieser A, Taft RW. 1968. *Progress in Physical Organic Chemistry*. New York: Wiley & Sons
44. Parr RG, Yang W. 1989. *Density Functional Theory of Atoms and Molecules*. New York: Oxford Univ. Press
45. Khalil M, Demirdoven N, Tokmakoff A. 2004. Vibrational coherence transfer characterized with Fourier-transform 2D IR spectroscopy. *J. Chem. Phys.* 121:362–73
46. Levine IN. 1978. *Physical Chemistry*. New York: McGraw-Hill
47. Pophristic V, Goodman L. 2001. Hyperconjugation not steric repulsion leads to the staggered structure of ethane. *Nature* 411:565–68
48. Bickelhaupt FM, Baerends EJ. 2003. The case for steric repulsion causing the staggered conformation of ethane. *Angew. Chem. Int. Ed. Engl.* 42:4183–88
49. Frauenfelder H, Parak F, Young RD. 1988. Conformational substates in proteins. *Annu. Rev. Biophys. Biophys. Chem.* 17:451–79
50. Frauenfelder H, Sligar SG, Wolynes PG. 1991. The energy landscapes and motions of proteins. *Science* 254:1598–603
51. Austin RH, Beeson K, Eisenstein L, Frauenfelder H, Gunsalus IC, Marshal VP. 1974. Activation-energy spectrum of a biomolecule: photodissociation of carbonmonoxy myoglobin at low temperatures. *Phys. Rev. Lett.* 32:403–5
52. Schnell JR, Dyson HJ, Wright PE. 2004. Structure, dynamics, and catalytic function of dihydrofolate reductase. *Annu. Rev. Biophys. Biomol. Struct.* 33:119–40
53. Oliveberg M, Wolynes PG. 2005. The experimental survey of protein-folding energy landscapes. *Q. Rev. Biophys.* 38:245–88
54. Ansari A, Berendzen J, Braunstein D, Cowen BR, Frauenfelder H, et al. 1987. Rebinding and relaxation in the myoglobin pocket. *Biophys. Chem.* 26:337–55
55. Tian WD, Sage JT, Champion PM. 1993. Investigation of ligand association and dissociation rates in the "open" and "closed" states of myoglobin. *J. Mol. Biol.* 233:155–66
56. Müller JD, McMahon BH, Chen EYT, Sligar SG, Nienhaus GU. 1999. Connection between the taxonomic substates of protonation of histidines 64 and 97 in carbonmonoxy myoglobin. *Biophys. J.* 77:1036–51
57. Li TS, Quillin ML, Phillips GN Jr, Olson JS. 1994. Structural determinants of the stretching frequency of CO bound to myoglobin. *Biochemistry* 33:1433–46
58. Vojtechovsky J, Chu K, Berendzen J, Sweet RM, Schlichting I. 1999. Crystal structures of myoglobin-ligand complexes at near atomic resolution. *Biophys. J.* 77:2153–74
59. Johnson JB, Lamb DC, Frauenfelder H, Müller JD, McMahon B, et al. 1996. Ligand binding to heme proteins. 6. Interconversion of taxonomic substates in carbonmonoxymyoglobin. *Biophys. J.* 71:1563–73
60. Teeter MM. 2004. Myoglobin cavities provide interior ligand pathway. *Protein Sci.* 13:313–18
61. Tilton RF Jr, Kuntz ID Jr, Petsko GA. 1984. Cavities in proteins: structure of a metmyoglobin-xenon complex solved to 1.9 Å. *Biochemistry* 23:2849–57
62. Doukov TI, Blasiak LC, Seravalli J, Ragsdale SW, Drennan CL. 2008. Xenon in and at the end of the tunnel of bifunctional carbon monoxide dehydrogenase/acetyl-CoA synthase. *Biochemistry* 47:3474–83

Annual Review of
Physical Chemistry
Volume 60, 2009

Contents

Indexes

Errata

An online log of corrections to *Annual Review of Physical Chemistry* articles may be found at http://physchem.annualreviews.org/errata.shtml